# MID-AMERICA
## TRANSPORTATION CENTER

UNIVERSITY OF Nebraska Lincoln

THE UNIVERSITY OF IOWA

KU THE UNIVERSITY OF KANSAS

MISSOURI S&T

LINCOLN UNIVERSITY MISSOURI

NICC NEBRASKA INDIAN COMMUNITY COLLEGE

UNIVERSITY OF Nebraska Omaha

University of Nebraska Medical Center

KU MEDICAL CENTER The University of Kansas

# Investigation of Wind Effects on Bridges Induced by Tornadoes for Tornado-Resistance Design - Phase II

## Grace Yan, PhD
Associate Professor
Department of Civil, Architectural and
Environmental Engineering
Missouri University of Science and
Technology

MISSOURI S&T

2024

Investigation of Wind Effects on Bridges Induced by Tornadoes
for Tornado-Resistance Design - Phase II

Grace Yan, PhD
Associate Professor
Department of Civil, Architectural and
Environmental Engineering
Missouri University of Science and
Technology

A Report on Research Sponsored by


Mid-America Transportation Center

University of Nebraska–Lincoln


July 2024

**Technical Report Documentation Page**

| 1. Report No.<br>25-1121-0005-039-2 | 2. Government Accession No. | 3. Recipient's Catalog No. |
|---|---|---|
| 4. Title and Subtitle<br><br>Investigation of Wind Effects on Bridges Induced by Tornadoes for Tornado-Resistance Design – Phase II | | 5. Report Date<br>January 15, 2022 |
| | | 6. Performing Organization Code |
| 7. Author(s)<br>Guirong Yan and Zhi Li | | 8. Performing Organization Report No.<br>25-1121-0005-039-2 |
| 9. Performing Organization Name and Address<br>Mid-America Transportation Center<br>Prem S. Paul Research Center at Whittier School<br>2200 Vine St.<br>Lincoln, NE 68583-0851 | | 10. Work Unit No. (TRAIS) |
| | | 11. Contract or Grant No. |
| 12. Sponsoring Agency Name and Address<br>Office of the Assistant Secretary for Research and Technology<br>1200 New Jersey Ave., SE<br>Washington, D.C. 20590 | | 13. Type of Report and Period Covered<br>January 2020-November 2021 |
| | | 14. Sponsoring Agency Code<br>MATC TRB RiP No. 91994-53 |
| 15. Supplementary Notes | | |

16. Abstract
Tornadoes have destroyed or severely damaged a number of bridges in the USA. Considering that tornadic wind loads have not been considered as a design load in the latest version (the 8th Edition, published in 2017) of the AASHTO Bridge Design Specifications, in Phase I of this project starting in January 2019, the PI has been characterizing the wind effects induced by tornadoes on bridges. In fact, bridges do not normally experience large deformation and vibration during strong winds. That is, the bridge can be assumed to be rigid in the computational domain, and the wind pressure on the bridge can be determined without consideration of the wind-bridge interaction, which is suitable for short-span or middle-span bridges. This project (Phase II) is to characterize the wind effects induced by tornadoes on those bridges whose deformation and vibration are significant under strong winds. In this case, the wind-bridge interaction will be considered. This is suitable for long-span bridges, such as cable-stayed bridges and suspension bridges. The obtained research findings will be used to modify the equations for calculating the design wind pressure on bridges, preventing bridges from being severely damaged or destroyed during future tornado incidents.

| 17. ORCID No. of each Researcher | | 18. Distribution Statement | |
|---|---|---|---|
| 19. Security Classif. (of this report)<br>Unclassified | 20. Security Classif. (of this page)<br>Unclassified | 21. No. of Pages<br>30 | 22. Price |

## Table of Contents

# List of Figures

Disclaimer

The contents of this report reflect the views of the authors, who are responsible for the facts and the accuracy of the information presented herein. This document is disseminated in the interest of information exchange. The report is funded, partially or entirely, by a grant from the U.S. Department of Transportation's University Transportation Centers Program. However, the U.S. Government assumes no liability for the contents or use thereof.

Abstract

Tornadoes have destroyed or severely damaged several bridges in the USA. Considering that tornadic wind loads have not been considered as a design load in the latest version (the 8th Edition, published in 2017) of the AASHTO Bridge Design Specifications, Phase I of this project, starting in January 2019, characterized the wind effects induced by tornadoes on bridges that do not normally experience large deformation and vibration during strong winds. That is, the bridge can be assumed to be rigid in the computational domain, and the wind pressure on the bridge can be determined without consideration of the wind-bridge interaction, which is suitable for short-span or middle-span bridges. This project (Phase II) aims to characterize the wind effects induced by tornadoes on bridges whose deformation and vibration are significant under strong winds. In this case, the wind-bridge interaction will be considered. This is suitable for long-span bridges, such as cable-stayed and suspension bridges. The obtained research findings will be used to modify the equations for calculating the design wind pressure on bridges, preventing bridges from being severely damaged or destroyed during future tornado incidents.

Chapter 1 Research Motivation and Research Objective

1.1 Research Motivation

Tornadoes, one of the most dangerous natural hazards, are a kind of non-synoptic wind phenomenon that regularly strikes the United States. Tornado outbreaks in inhabited regions have resulted in severe property damage, injuries, and fatalities. At least 695 people lost their lives in the deadliest tornado in US history, the Tri-State tornado, which struck on March 18, 1925 [1]. The Oklahoma tornado on May 3, 1999 had the greatest recorded wind speed of $302 \pm 22$ mph ($486 \pm 35$ km/h), resulting in \$1.5 billion in damages and the deaths of 36 people [2]. The Joplin tornado on May 22, 2011 killed 162 people and caused \$2.8 billion of property loss [3]. Due to the significant loss of lives and properties, the incorporating of a tornado-resistant design into buildings has gained widespread acceptance. The specifications of a tornado-resistant design for Risk Categories III or IV buildings have been incorporated in a new chapter in ASCE 7-22, Chapter 32.

Section 3.8 in AASHTO, "Wind Load", governs the wind design for bridges. Due to a lack of tornado-resistant bridge design, 13 bridges in the USA were destroyed or badly damaged by tornadoes (see Figures 1.2-1.5). For instance, on July 21, 2003, a low-intensity tornado (rated as F-1) demolished the railroad bridge that crossed the Kinzua gorge [4]. Of its twenty towers, eleven were demolished, as illustrated in Figure 1.2. The wind speed at that moment was only 73–112 mph. Given that the bridge was demolished at such a low wind speed, it seems likely that the damage was a result of tornadoes' distinct wind effects that differ from straight-line winds— that is, swirling, rotating winds. Consequently, understanding how tornadoes impact bridges is essential to inform a tornado-resistant design for bridges.

Figure 1.1 A tornado



Figure 1.2 Kinzua bridge (F1 tornado in 2003)



Figure 1.3 Utica Swing Bridge, 1906



Figure 1.4 New Castle Bridge, 2013
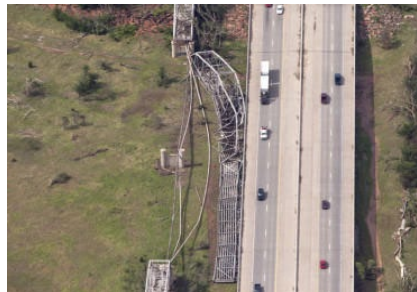


Figure 1.5 Hurricane Creek Bridge, 2011, F4
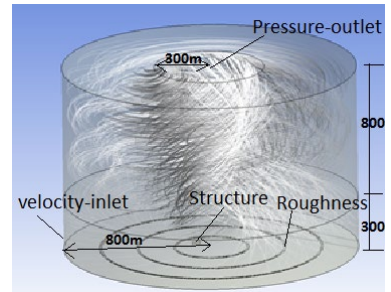


Figure 1.6 Simulated tornadic wind field

## 1.2 Research Objective

A thorough literature review revealed that while much research has been done on the tornadic wind effects on other types of structures and straing-line wind effects on bridges, the wind effects caused by tornadoes on bridges have not yet been well studied [5,6,7,8,9,10,11,12,13,14,15]. This is especially true for long-span bridges, such as cable-stayed bridges. The goal of this project is to provide understanding of tornadic wind effects on cable-stayed bridges using CFD simulations, which can be used to enhance bridge wind resistance and prevent catastrophic failure of cable-stayed bridges during tornadoes. This will be achieved by applying CFD simulations. To modify the wind pressure equation provided in AASHTO, the CFD model simulates the action of an equivalent straight-line wind field on the cable-stayed

bridge. A modified formula for determining the design wind pressure for a tornado-resistant design for cable-stayed bridges in the AASHTO Bridge Design Specifications is one of the anticipated outcomes and outputs. The obtained design tornadic wind loads can be utilized to determine how vulnerable current bridges are and to create a strategy for reinforcing them to resist a certain intensity of tornado.

1.3 Description of the Bridge of Interest

The study considers the wind effects on a cable-stayed bridge with the length of 274.32 meters and the width of 12.19 meters. The bridge model is created and constructed using Pointwise. Figure 1a) presents the 3D model of this cable-stayed bridge. The Pointwise model of this bridge is presented in Figure 1b). The zoomed-in image of the red circle area in Figure 1b), shown in Figure 1c), provides details about the diaphragm plates and I-shaped girders.
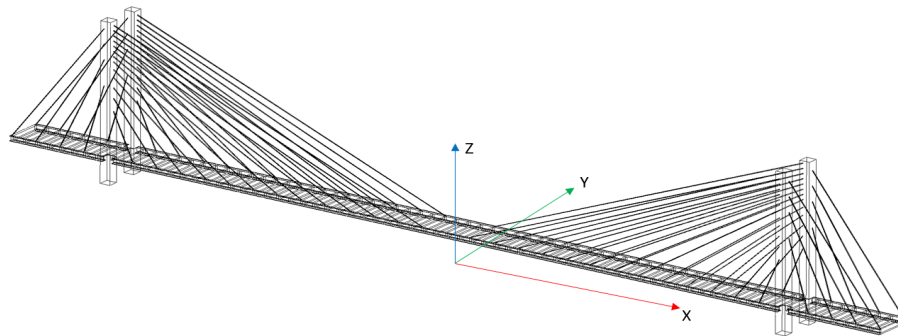


a) 3D model of the cable-stayed bridge
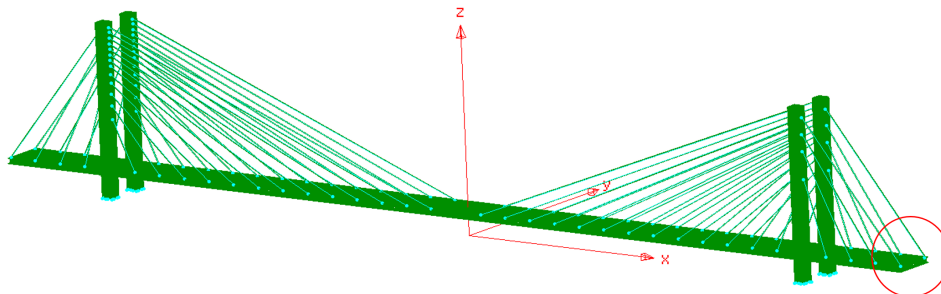


b) The model of the cable-stayed bridge established in Pointwise

3
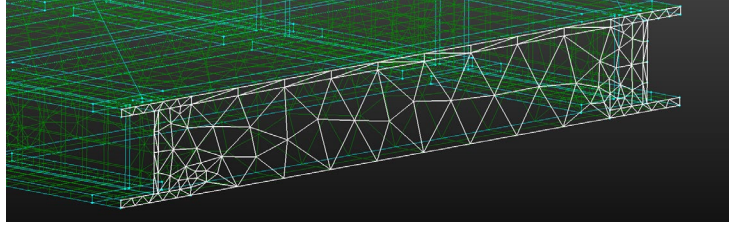
c) Cross section of the bridge deck
Figure 1.7 The Model of the cable-stayed bridge

1.4 Research Tasks

The following three tasks have been carried out to address the proposed research objective. First, a real-world tornado was simulated and the wind effects of tornadoes on the cable-stayed bridge were obtained, as detailed in Chapter 2. Second, the equivalent straight-line wind field was simulated, and the wind effects on the cable-stayed bridge under the equivalent straight-line winds was obtained and compared with those under tornadic winds, as detailed in Chapter 3. Third, the obtained results from Chapters 2 and 3 were used to modify the equation in Chapter 4 of the AASHTO code for determining the design wind pressure for cable-stayed bridges. Fourth, Chapter 5 presents conclusions and future work.

Chapter 2 Simulation of Tornadic Wind Field and Investigation of Wind Effects of Tornadoes on the Cable-stayed Bridge

This chapter describes how a real-world tornado in Spencer, SD on May 30, 1988, was simulated at full-scale and how to obtain the tornadic wind effects on the cable-stayed bridge. First, only the pure wind field was simulated, to confirm that the simulated tornadic wind field was accurate. Second, the cable-stayed bridge introduced in Section 1.3 was incorporated within the computational domain and the wind effects were extracted during the entire duration when the tornado passed the bridge.

2.1 CFD Simulation Setup

A cylindrical computational domain was applied to simulate swirling air flow. It is a comprehensive simulation, as illustrated in Figure 2.1. The radius of the pressure outlet is 340 meters, while the height of the velocity inlet is 100 meters. The velocity-inlet is the inflow surface boundary condition, and the pressure-outlet is the outflow surface boundary condition in this computational domain. All other boundaries were set as non-slip walls. A fine mesh was used in the center of the convergent zone and the area close to the ground.

Large Eddy Simulation (LES), which is controlled by filtered time-dependent Navier-Stokes equations, serves as the foundation for the CFD simulation. Large eddies are assumed to be the primary means of transporting mass and momentum and can be solved directly from the equations, while small eddies are represented numerically using the WALE (Cwale = 0.325) sub-grid model (Nicoud and Ducros, 1999). Since the SIMPLEC (Semi-implicit hand for Pressure Linked Equation) scheme often has better convergence than PISO (Pressure-Implicit with Splitting of Operators), the segregated implicit solver is used to solve the governing equation using a SIMPLEC approach for pressure-velocity coupling [16].

The simulation is initially performed for 260 s to produce a stationary tornadic wind field. To replicate the tornado's translation, a relative motion is created between the bridge and the computational domain's ground surface by moving the bridge in the opposite direction from the tornado's translation, but at the same speed, which in this case is 15 m/s. To simulate the translation stage of the tornado, an additional 68 seconds were simulated with the layering approach of the dynamic meshing method. The time step of this simulation was set as 0.01 s. After meshing, the domain had about 10 million cells, which includes the cable-stayed bridge.

2.2 Velocity Input

The velocity input at the velocity inlet was defined in Eqs. (2.1), (2.2), and (2.3). They are the tangential velocity profile and the radial velocity profile along height, which are the regression equations of the radar-measured velocity data at a radius of 800 m of the Spencer, SD tornado of 30 May 1988 [17]. All other boundary conditions are defined as symmetry.

$$\text{Tangential velocity: } V_t = 20.61(Z/20)^{0.1774} \tag{2.1}$$

$$\text{Radial velocity: } V_r = -31.34\left(\frac{Z}{20}\right)^{0.169} \qquad Z \leq 20\ m \tag{2.2}$$

$$V_r = 45.14\left(\frac{Z}{20}\right)^{0.1826} - 76.48 \qquad Z \geq 20\ m \tag{2.3}$$

where Z is the height from the ground surface.
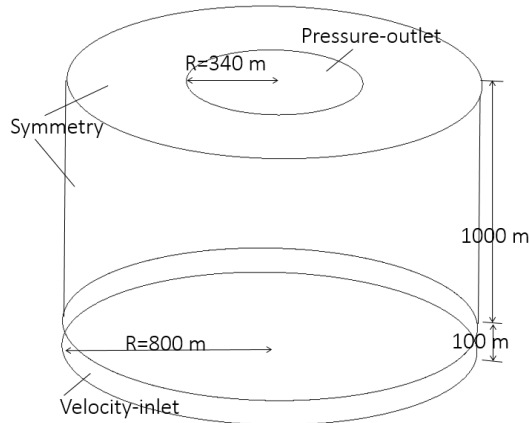
Figure 2.1 Computational domain of the tornadic wind field

2.3 Validation of the simulated tornadic wind field

The CFD model of the tornadic wind field was verified using the velocity data obtained from radar measurements. As indicated by the red graph in Figure 2.2, the tangential velocity profile along the radius at an elevation of 80 meters was extracted and displayed. The time-averaged tangential velocity is calculated during from 260–300 seconds. The tangential velocity profile extracted from the radar-measured velocity data of the Spencer, SD tornado was also displayed in Figure 2.2, as indicated by the black graph. The two graphs are very close to each other, with similar maximum tangential velocity and core radius, validating the CFD model.


Figure 2.2 Tangential velocity profile along the radial distance at the elevation of 80 m

7

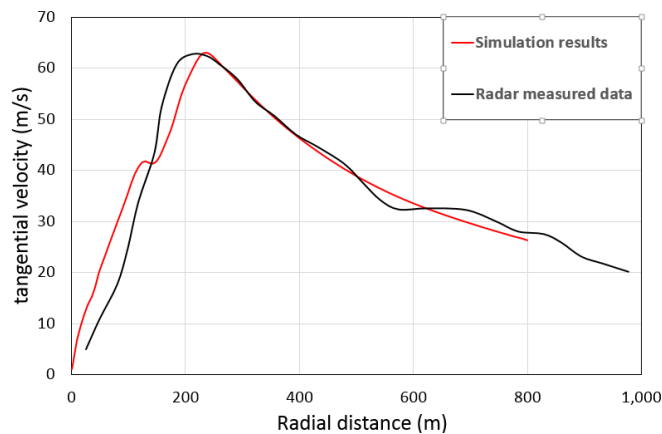The instantaneous tangential velocity distribution at 270 s on an 80 m horizontal plane is shown in Figure 2.3. The arrows show the direction of the resultant velocity of tangential and radial velocity components, while the color indicates the tangential velocity magnitude. With increasing tangential velocity, the wind flow outside the core region converges towards the tornado center. After reaching its greatest value at a particular radius known as the core radius, the tangential velocity then decreases along the radial distance from the core radius to the tornado center.

At around the core radius, the tangential velocity forms circular strips with uniform velocities in each strip. There is only one vortex in this tornado, as seen in Figure 2.3. The tangential velocity distribution through the tornado center on a vertical plane is shown in Figure 2.4. The arrows show the direction of the resultant radial and vertical component velocities, while the color indicates the tangential velocity magnitude. Updrafts are seen in the surrounding areas, and a downdraft is seen in the center, demonstrating the double-celled, single-vortex flow structure.

The instantaneous pressure contour on the horizontal plane at an elevation of 80 meters is shown in Figure 2.5. Regular circular strips are observed. The instantaneous pressure contour through the tornado core on a vertical plane is shown in Figure 2.6. On both the horizontal plane and the vertical plane, it shows that pressure drops steadily from the periphery to the center.
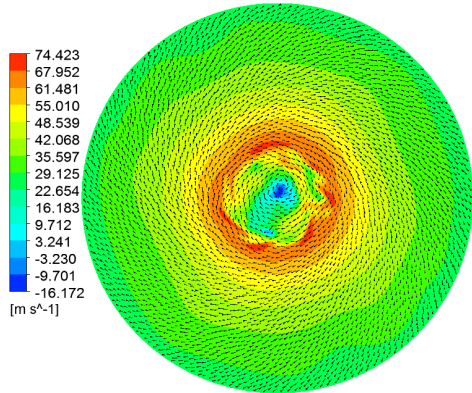
Figure 2.3 Instantaneous Tangential velocity distirbuition on the horizontal plane at the elevation of 80 m
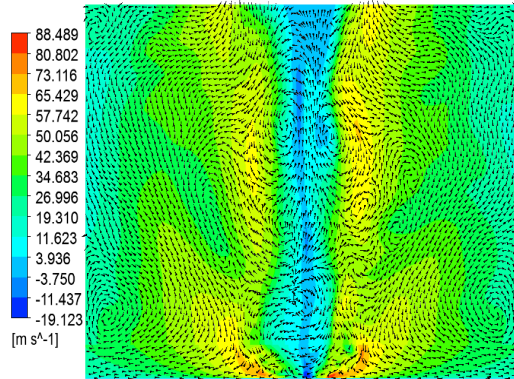


Figure 2.4 Instantaneous Tangential velocity on a vertical plane through tornado center
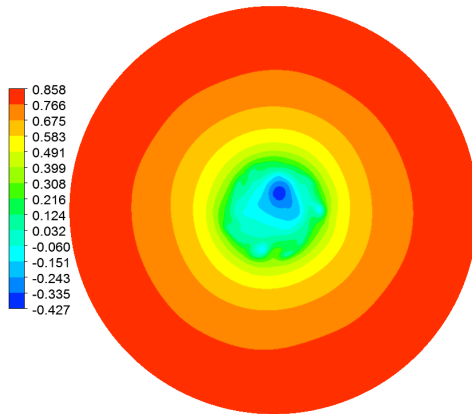


Figure 2.5 Instantaneous Pressure distribution on the horizontal plane at the elevation of 80 m
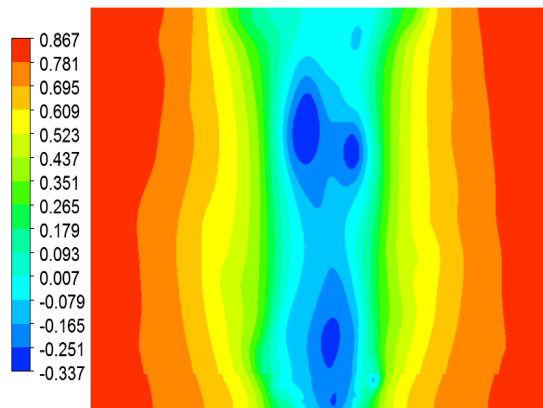


Figure 2.6 Instantaneous Pressure distribution on a vertical plane throuth tornado center

## 2.4 Wind Effects Induced by the Tornado on the Cable-stayed Bridge

To obtain the wind effects on the cable-stayed bridge, this bridge is included in the tornadic wind field (see Figure 2.7). The pressure coefficient is adopted to represent the pressure distribution on the bridge surface. In this study, the pressure coefficient is calculated based on Eq. (2.4)

$$C_p = \frac{P - P_r}{\frac{1}{2}\rho_r V_r^2} \qquad (2.4)$$

where $P - P_r$ denotes the relative static pressure at the point where the pressure coefficient is evaluated. $P_r$, $V_r$, and $\rho_r$ denote the reference pressure, reference wind velocity, and air density, respectively, which are $P_r = 101{,}325$ Pa, $V_r = 81.1$ m/s and $\rho_r = 1.225$ kg/m$^3$ in this study [17].
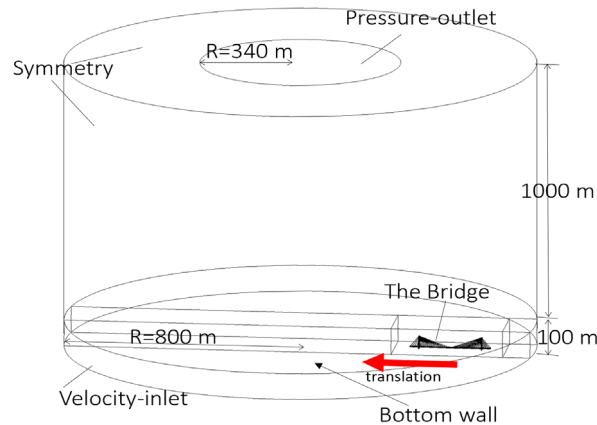


Figure 2.7 Tornadic wind field with the cable-stayed the bridge included

Figure 2.8 shows the extracted instantaneous tangential velocity and pressure distribution on the horizontal plane at an elevation of 6.85 meters. At this point, the center of the computational domain is closer to the center of the cable-stayed bridge. Figures 2.8a) and 2.8c) show the stream lines of the wind flow as black graphs. At this moment, it is difficult to pinpoint the exact center of the tornado because of the cable-stayed bridge. When compared to the wind flow outside the core radius, the wind flow inside the core radius is more turbulent and moves at a slower speed. Figure 2.8 b) shows the instantaneous pressure distribution on the horizontal plane at an elevation of 6.85 m. Outside the core region, regular circular strips are observed, and the pressure magnitude steadily falls along the radius from the outside region to the center of the tornado, following the typical features of tornadoes. The presence of the bridge results in

multiple dark blue, lower-pressure patches in the core region, illustrating variations in the

pressure distribution that occur, which is different from the pure wind field (when a tornadic

wind field does not have any structure). The zoomed-in image of the indicated location in Figure

2.8b) is shown in Figure 2.8c). There are a number of tiny vortices visible between the

diaphragm plates under the bridge's deck and on both sides of the pylon.

      As illustrated in Figure 2.9, the pressure coefficient operating on the cable-stayed bridge

is extracted as its center gets closer to the computational domain center. Due to the air pressure

drop in the tornado's center, negative pressure predominates the bridge. On the side of the I-

shaped girder at the end of the bridge, which is shown by a red circle, positive pressure is seen.

This is due to the bridge's end experiencing a high horizontal velocity as it approaches the core

radius.
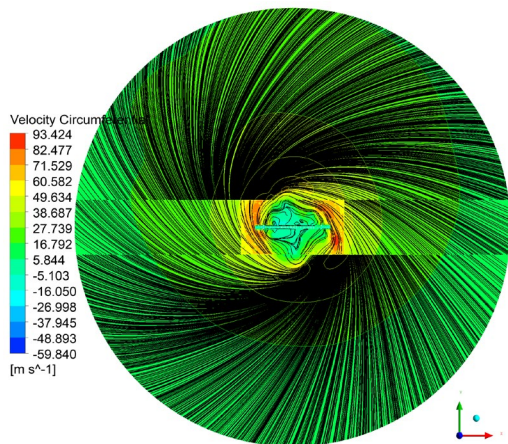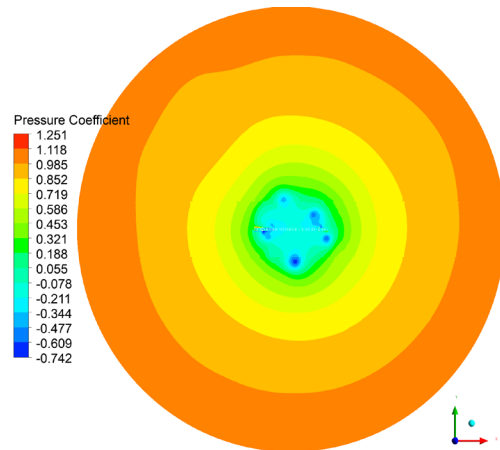


a) Tangential velocity distribution on the     b) Pressure distribution on the horizontal plane
horizontal plane
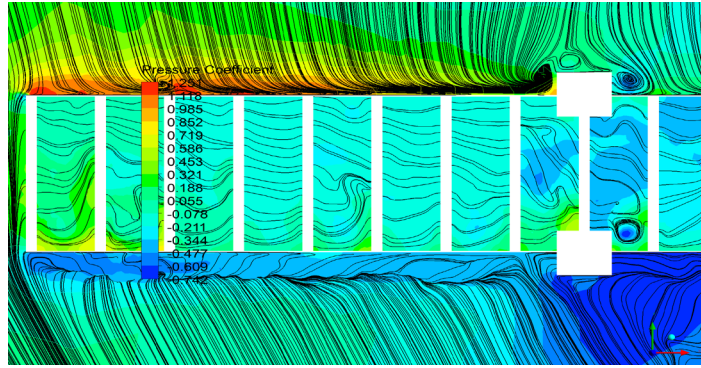
c) Zoom-in picture of the marked region

Figure 2.8 Pressure and tangential velocity distribution on the horizontal plane
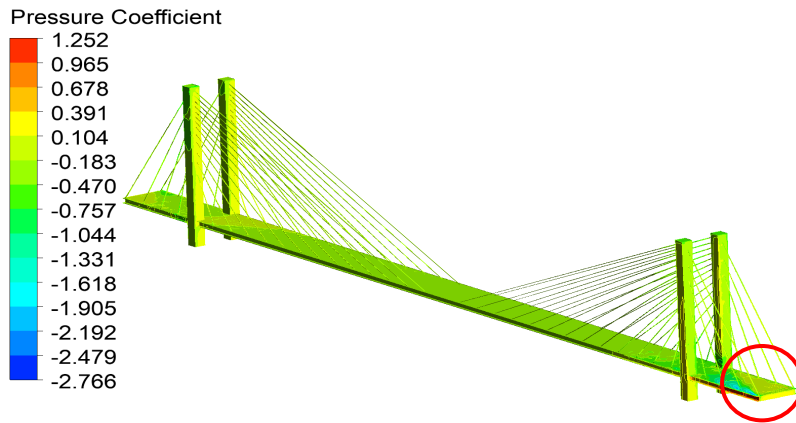at the elevation of 6.85m



Figure 2.9 Pressure coefficients acting on the cable-stayed bridge when the bridge approaches
the center of the computational domain

Chapter 3 Wind Effects of Equivalent Straight-line Winds on the Bridge and Its Comparison with Tornadic Wind Effects

An equivalent straight-line wind field is constructed to acquire the wind effects generated by straight-line winds, because the existing AASHTO wind design is based on straight-line winds. The coefficients in the wind pressure equation (in AASHTO) can be changed to compute the wind pressure created by tornadoes by comparing the wind effects caused by tornadic winds and its equivalent straight-line winds. The equivalent straight-line wind field is simulated in this chapter. The cable-stayed bridge is placed in this straight-line wind field to examine the wind effects of straight-line winds on the bridge (refer to Figure 3.1). The method used by Franke (2006) [18] was applied to determine the size of this rectangular computing domain.
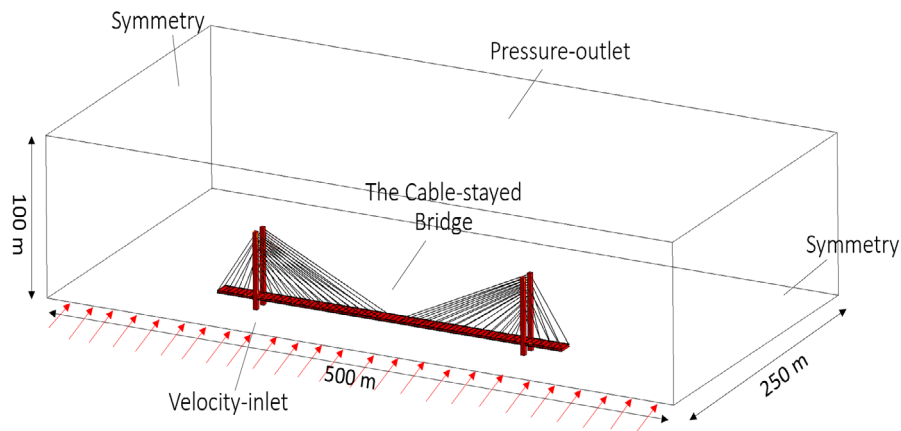


Figure 3.1 Equivalent straight-line wind field including the cable-stayed bridge

3.1 Simulation Setup

The computational domain of the straight-line wind field is designed according to Franke (2006) [18]. The distances between the velocity-inlet or pressure-outlet boundaries and the cable-stayed bridge are 5H and 15H, respectively, where H is the height of the cable-stayed bridge's deck. The blockage ratio is 1.4%, which satisfies the requirement of the straight-line wind tunnel

test. The velocity input is based on a power-law profile and the exponent of the power-law is 0.14, as shown in Eq. (3.1), which is to simulate the scenario of the open terrain. The maximum resultant velocity (the resultant velocity of tangential and radial velocities) at the height of cable-stayed bridge's deck ($H_r$= 6.85 m) is 81.1 m/s in the tornadic wind field. Therefore, the velocity profile applied to the velocity input is expressed below.

$$V_s = 81.1(Z/H_r)^{0.14} \qquad\qquad (3.1)$$

where $V_s$ denotes the velocity at different heights; $H_r$ denotes the reference height ($H_r$= 6.85 m) and Z denotes the height above ground.

K, or turbulent intensity, is used as the Reynolds Stress Specification technique for the equivalent straight-line winds, where the turbulent intensity is 10% and the turbulent viscosity ratio is 0.01. Thirty-six seconds of simulation is run, with a time step of 0.01 s. With the cable-stayed bridge included, the equivalent straight-line wind field has a total of about 9.8 million cells.

3.2 Comparison of the peak velocity on horizontal plane and peak pressure on bridge surface induced by tornadic winds and the equivalent straight-line winds

Figure 3.2 shows the outcome of the 3-second time-averaged velocity distribution along the Y direction on the horizontal plane. The streamlines of flow, represented by the black lines on both sides, remain straight on the horizontal plane, with the exception of the area near the cable-stayed bridge. This suggests that the straight-line wind field's design is appropriate because the wind flow is not impeded by the wind field's boundary. When the air approaches the cable-stayed bridge, the velocity increases, as the wind flow must accelerate due to the blockage of the cable-stayed bridge. The maximum negative velocity is noted where vortices occur at the

corners close to the pylons on the windward side. When comparing the maximum tangential velocity, the magnitude under tornadic winds (93 m/s; see Figure 2.8 a)) is slightly greater (4%) than that under the equivalent straight-line winds (89 m/s, see Figure 3.2).

The 3-second time-averaged pressure distribution on the horizontal plane at an elevation of 6.85 meters is shown in Figure 3.3 a). With the exception of the areas close to the cable-stayed bridge, the pressure distribution is uniform on the horizontal plane. The windward side of the cable-stayed bridge experiences the highest positive pressure. According to the Bernoulli equation, the flow velocity drops to zero at the stagnation point on the windward side, and the pressure rises as a result. The magnified image of the red-marked area in Figure 3.3 a) is shown in Figure 3.3 b). The streamlines in the wind field are represented by black lines in Figure 3.3 b). The two corners of the pylon on the windward side of the cable-stayed bridge are where the greatest negative pressures are found. On the leeward side of the bridge, two large vortices are observed behind the pylon. On the windward side of the cable-stayed bridge and in the spaces between the diaphragm plates beneath the bridge deck, tiny vortices are also observed. Hence, negative pressure predominates the area beneath the bridge deck, which causes suction. When compared to the tornadic case, as depicted in Figure 2.8 c), the big vortices vanish and the quantity of vortices is lower than under straight-line winds, indicating the differences in wind flow between tornadic and straight-line winds, even though the wind flow under tornadic winds moves similarly to the straight-line winds in the marked region.

Figure 3.4 shows the pressure distribution on the cable-stayed bridge's surface. Negative pressure predominates the cable-stayed bridge's surface. Only the pylons and the windward side of the deck exhibit positive pressure. The red circle indicates the top section of the pylons, where the highest positive pressure is observed. These findings resemble those of Erdem (2016) [19].

Erdem came to the conclusion that the tower's vertical surface experienced the greatest pressure

distribution, which rose in direct proportion to the tower's height. Because the wind must speed

up to pass through the pylons, the highest negative pressure is achieved on their sides. According

to the Bernoulli equation, pressure decreases as velocity increases. The point of greatest pressure

is not the same as the point during tornadic winds. The maximum positive pressure in the

tornadic situation (see Figure 2.9) is found on the windward side of the I-shaped beam, and the

maximum negative pressure is found at the deck corner closest to the area experiencing the

maximum positive pressure. The maximal negative pressure magnitude (2.766) under tornadic

winds is 12% larger than that under the equivalent straight-line winds (2.466), as depicted in
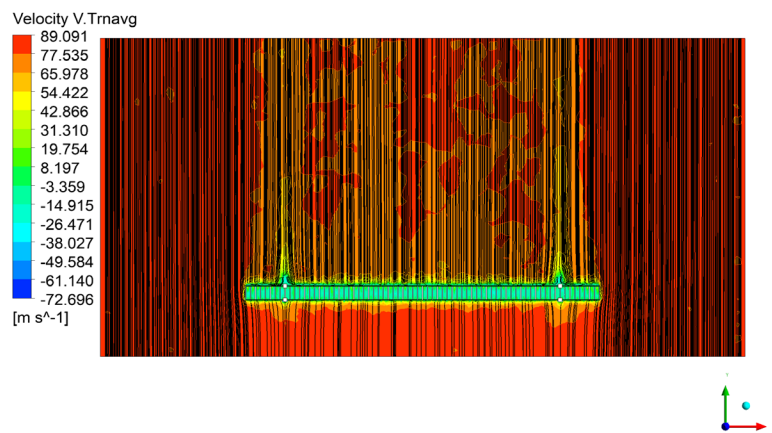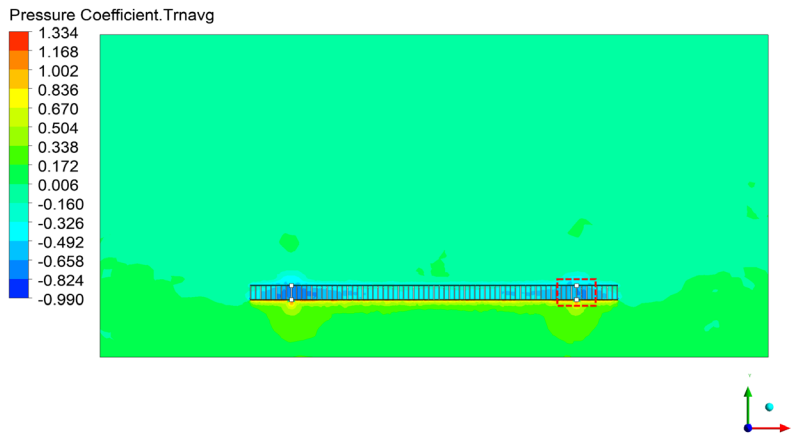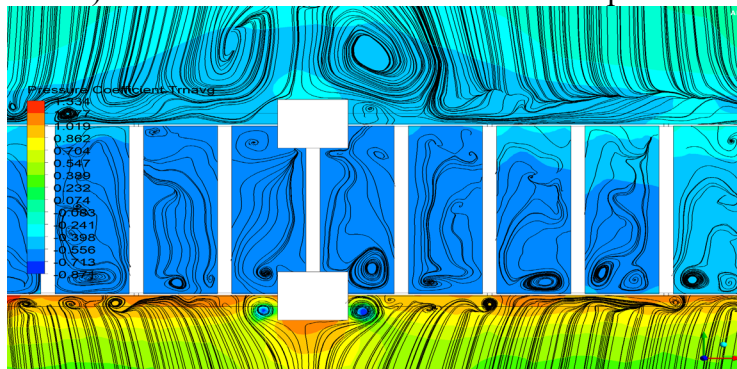
Figure 3.4.



Figure 3.2 Time-averaged velocity distribution on the horizontal plane at the elevation of
6.85m

a) Pressure distribution on the horizontal plane



b) Zoom-in picture of the marked region

Figure 3.3 Time-averaged pressure distribution on the horizontal plane
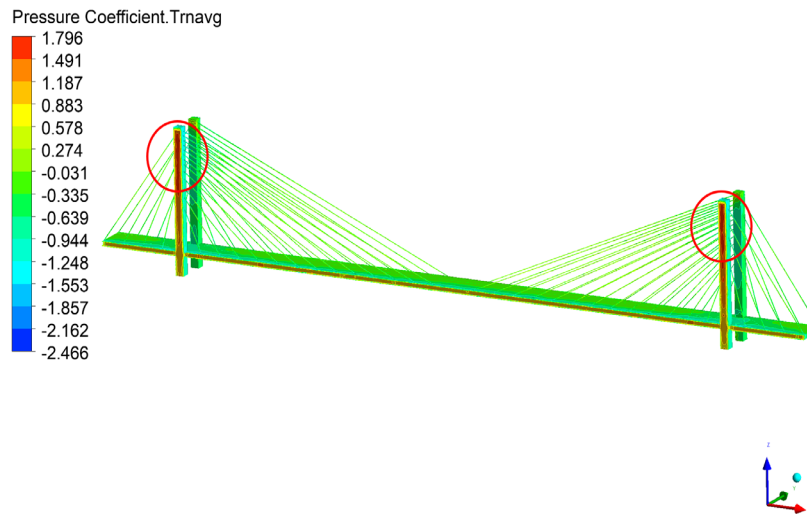at the elevation of 6.85m



Figure 3.4 Time-averaged pressure distribution on the surface of the cable-stayed bridge
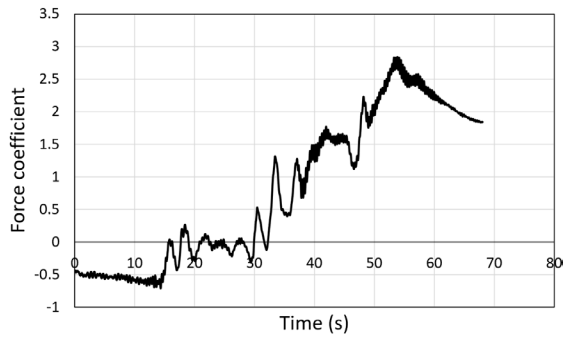
3.3 Comparison of the force and moment coefficients acting on the cable-stayed bridge under tornadic winds and under the equivalent straight-line winds

The force coefficients acting on the cable-stayed bridge under tornadic winds (see Figure 3.5) and the equivalent straight-line winds (see Figure 3.6) are extracted and compared. The temporal history of the force coefficient operating on the cable-stayed bridge exhibits notably distinct tendencies when comparing Figures 3.5 and 3.6. The two peak values at the designated time instants, which are approximately 15 s and 50 s, are shown. At these two time instants, the cable-stayed bridge's center gets closer to the tornado's core radius, where it is exposed to extremely high wind velocity. In the vicinity of the core radius, the force coefficient exhibits dense and tiny fluctuations, but expands in a large magnitude range. The force coefficient on the bridge under the equivalent straight-line winds, however, exhibits random fluctuation in a narrow magnitude range, as illustrated in Figure 3.6. This indicates that the wind flow in the straight-line wind field is more stable than in the tornadic wind field.

Within the computational domain, X is along the longitudinal direction of the cable-stayed bridge, Y is perpendicular to the bridge's longitudinal direction, and Z is in the vertical direction. The highest magnitude is always attained in the tornadic scenario, with the exception of the force coefficient in the Y direction, when comparing the force coefficient caused by tornadic winds to that caused by the equivalent straight-line winds. Because the wind flow in a straight-line wind field flows perpendicular to the X direction, the wind force is relatively small along the X direction, which is why the peak value of the force coefficient in the X direction under tornadic winds (2.8) is 11 times greater than that under straight-line winds (0.25). When tornadic winds are present, the force coefficient in the Z direction peaks at 0.25, which is 11 times higher than when straight-line winds are present (0.022). As a result, while designing a cable-stayed bridge to withstand tornadic winds, the wind design should increase the lift force.

On the other hand, the force coefficient peak value under straight-line winds (2.94) is 1.7 times higher in the Y direction than it is under tornadic winds (1.7). However, the maximum horizontal resultant force caused by tornadic winds is higher than that caused by the equivalent straight-line winds.
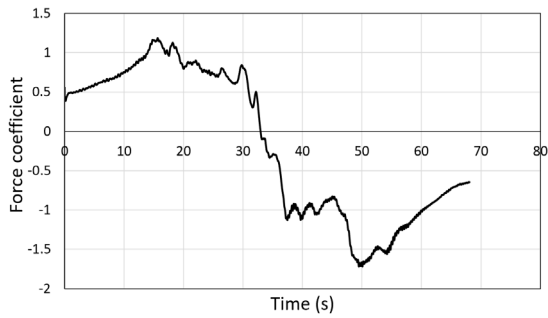
Figures 3.7 and 3.8 show the extracted moment coefficients acting on the cable-stayed bridge under tornadic winds and the corresponding straight-line winds. When the cable-stayed bridge is near the core radius, the time history of the moment coefficient about the X and Y axes under tornadic winds exhibits two peak values (see Figures 3.7 a) and b)). When the cable-stayed bridge gets closer to the tornado center, the moment coefficient about the Z axis only exhibits one peak value (see Figure 3.7 c)). The temporal history reveals sharp variations in the wind speed within the tornadic wind field, particularly as the cable-stayed bridge gets closer to the tornado's center and core radius. On the other hand, the time history for the cable-stayed bridge under straight-line winds reveals random fluctuations within a narrow magnitude range. The highest moment coefficient value about the X axis under tornadic winds (7) is 1.19 times smaller than under equivalent straight-line winds (8.35), as can be seen by comparing Figures 3.7 and 3.8. When tornadic winds are present, the moment coefficient's highest value about the Y axis (0.25) is 4.2 times higher than that when straight-line winds are present (0.06). Despite both being extremely small, the highest value of the moment coefficient about the Z axis under tornadic winds (0.09) is 27.3 times larger than that under the equivalent straight-line winds (0.0033).
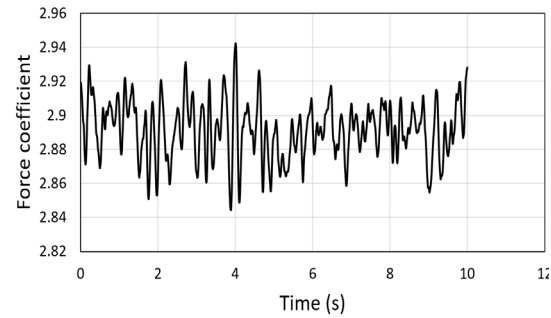
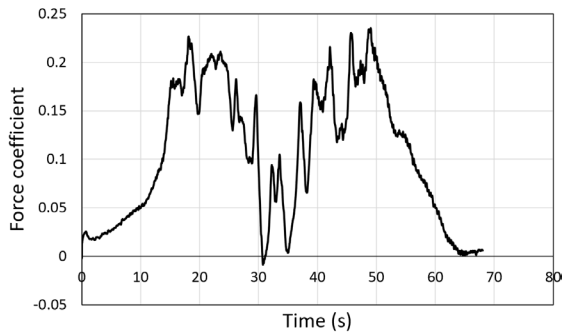a) Force coefficient in X direction
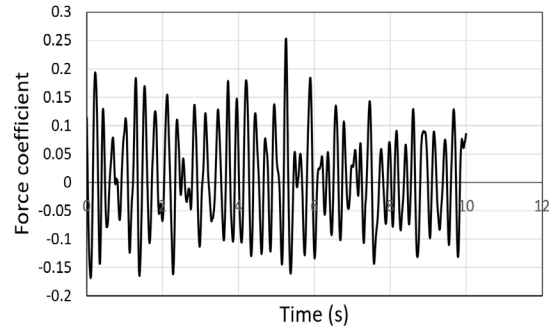


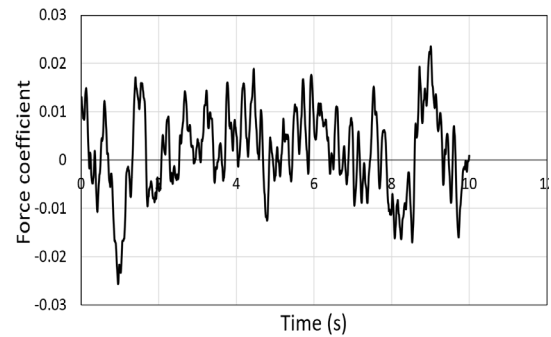a) Force coefficient in X direction



b) Force coefficient in Y direction



b) Force coefficient in Y direction



c) Force coefficient in Z direction



c) Force coefficient in Z direction

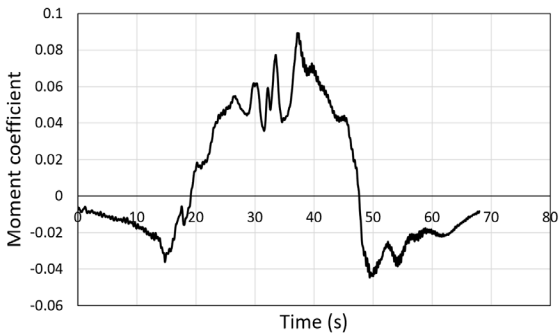Figure 3.5 Time history of the force coefficient acting on the cable-stayed bridge under tornadic winds

Figure 3.6 Time history of the force coefficient acting on the cable-stayed bridge under the equivalent straight-line winds

20

a) Moment coefficient about the X axis



a) Moment coefficient about the X axis



b) Moment coefficient about the Y axis
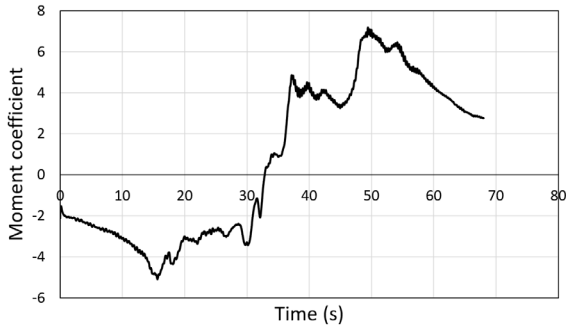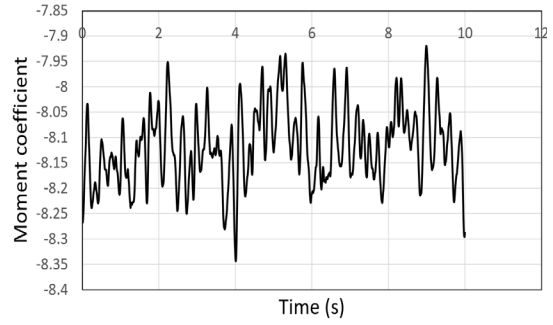


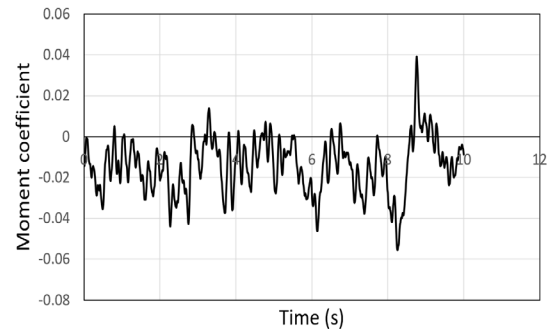b) Moment coefficient about the Y axis
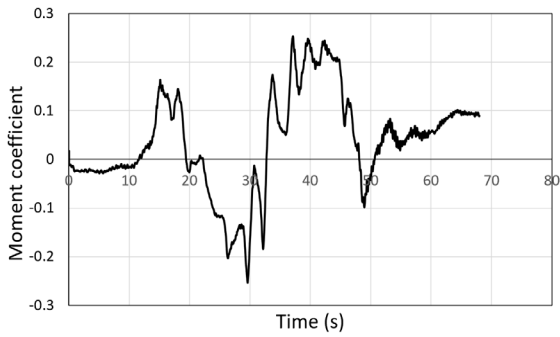


c) Moment coefficient about the Z axis



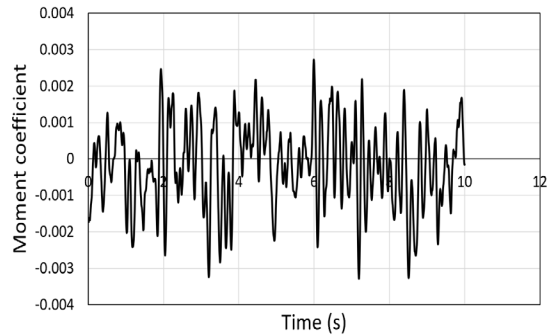c) Moment coefficient about the Z axis

Figure 3.7 Time history of moment coefficients acting on the cable-stayed bridge under tornadic winds

Figure 3.8 Time history of moment coefficient acting on the cable-stayed bridge under the equivalent straight-line winds

## 3.4 Force and moment coefficient acting on the unit length deck of the cable-stayed bridge under tornadic winds and under the equivalent straight-line winds

The accompanying structural analysis is performed using ANSYS mechanical 17.1 to examine the force and moment coefficients acting on the unit length (1 m) deck of the cable-stayed bridge. First, as seen in Figure 3.9 a), the finite element model (FEM) of the unit length deck of the cable-stayed bridge is constructed using the DesignModeler in the workbench. Second, using the transient load mapping technique (ANSYS 2013), the tornadic wind pressure acting on the surface of the cable-stayed bridge during the final 68 seconds of the simulation period (when the bridge moves) is mapped onto this FEM, as illustrated in Figure 3.9 c). This data is taken from the CFD simulation. As demonstrated in Figure 3.9 b), the fixed support boundary conditions are applied to both sides of the FEM to determine the force and moment exerted on it by the tornadic wind pressure. Lastly, the coefficients of force and moment operating on the FEM are computed. In addition to obtaining the force and moment coefficients acting on the FEM under tornadic winds, the process and methods are again employed to map the straight-line wind pressure onto the FEM.
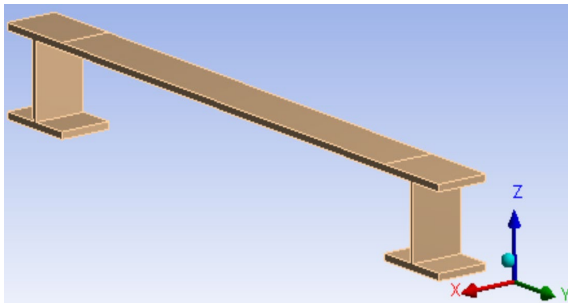
a) The FEM of the unit length deck of
the cable-stayed bridge
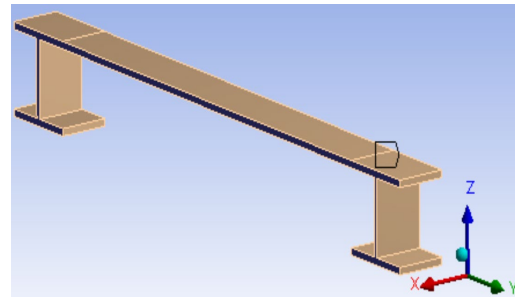
b) The FEM after adopting fixed support at
two sides

22
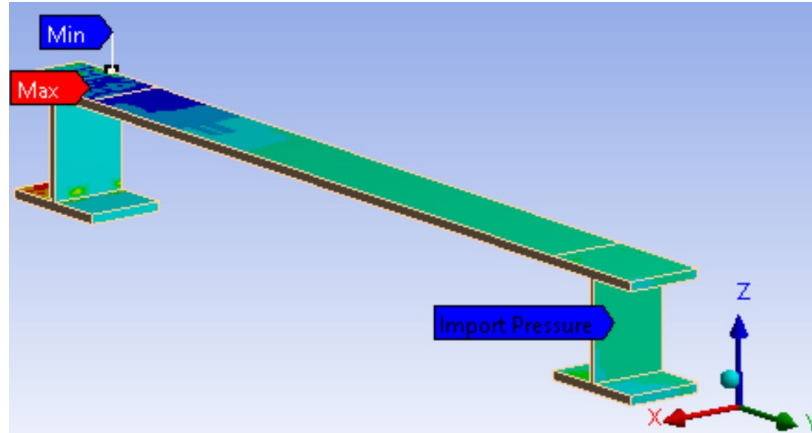
c) The FEM after importing the tornadic wind pressure onto the surface

Figure 3.9 FEM designed in ANSYS DesignModeler

As illustrated in Figure 3.10, the force coefficient acting on the FEM in the X direction (henceforth referred to as "Fx") is extremely tiny for the FEM under tornadic winds. This is because fixed support is supplied to these two sides, and no pressure is projected onto the surface perpendicular to the X direction. The force coefficients acting on the complete cable-stayed bridge (shown in Figures 3.5 b) and c) and in the Y and Z directions (referred to as "Fy" and "Fz") in Figures 3.10 b) and c) are similar. When FEM sequentially approaches the tornado's core radius, two peak values are seen. And the time instant at which the FEM finds the tornado's center, 30 s, yields the lowest value.

As can be seen in Figure 3.11 a), the FEM under corresponding straight-line winds results in a very tiny magnitude of Fx, which is comparable to the FEM under tornadic winds. Because of the relative stability of straight-line winds, Figures 3.11 b) and c) depict random fluctuation in a narrow range for the Fy and Fz coefficients.

The comparison of Fx under tornadic winds and their equivalent straight-line winds is not a valid reference because the Fx is extremely modest. The peak value of Fy under tornadic winds (1.9) is 1.08 times bigger than that under equivalent straight-line winds (1.75). Furthermore, the

23

FEM encounters more unfavorable conditions under tornadic winds, as indicated by the highest

value of Fz (0.34), which is 7.5 times greater than that under equivalent straight-line winds

(0.045).

In Figures 3.12 and 3.13, the time history of the moment coefficient is extracted and

displayed. Figures 3.12 a) and b) illustrate the moment coefficient about the X axis (Mx) and

about the y axis (My) under tornadic winds, which demonstrate the rapid change of wind impacts

on the FEM over time. The time history of Mx and My shows two peak values, which

correspond to the time instants t = 15s and 35s, because at these two time instants the FEM

experiences high velocity at the core radius; the smallest value happens at t = 25s when the FEM

is located at the tornado center. The time histories of Mx, My, and Mz for the FEM under the

equivalent straight-line winds exhibit random fluctuation within a narrow magnitude range,

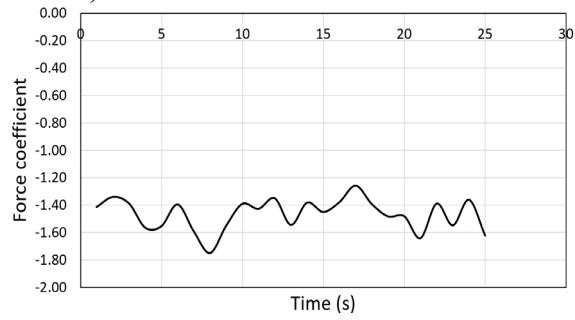indicating a rather steady wind flow in straight-line winds.
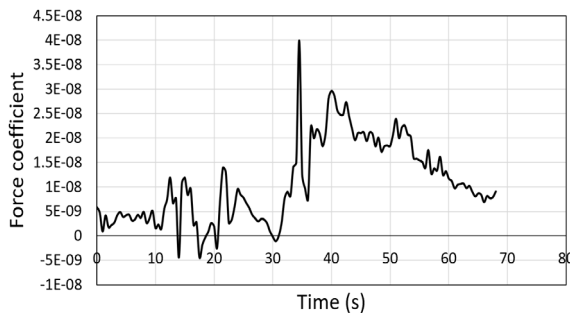


a) Force coefficient in X direction
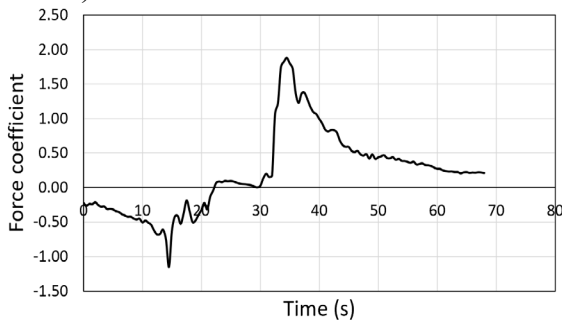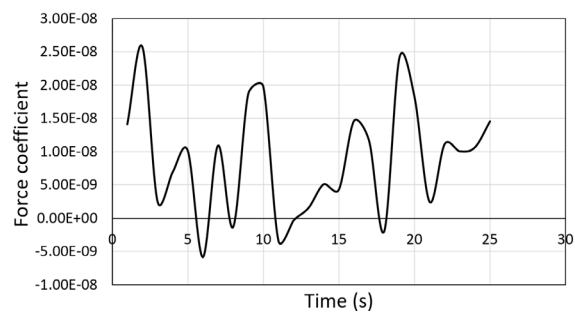


a) Force coefficient in X direction



b) Force coefficient in Y direction



b) Force coefficient in Y direction
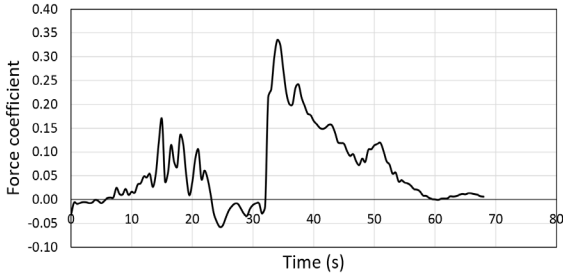
c) Force coefficient in Z direction

Figure 3.10 Time history of force coefficient acting on the FEM under tornadic winds
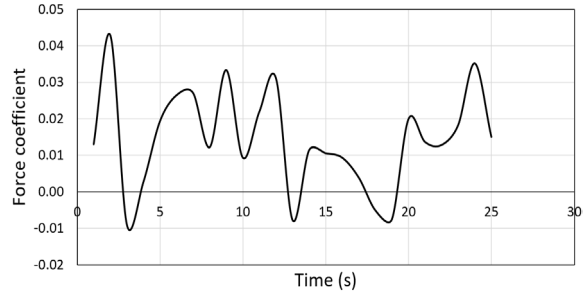


c) Force coefficient in Z direction

Figure 3.11 Time history of force coefficient acting on the FEM under the equivalent straight-line winds
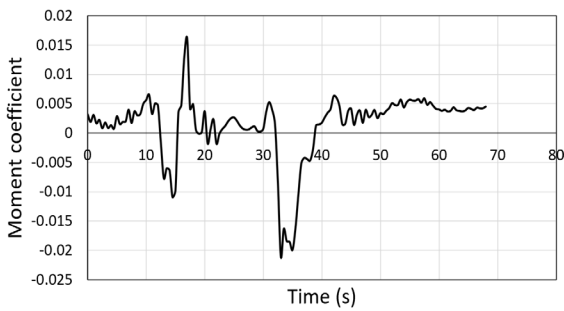


a) Moment coefficient about the X axis
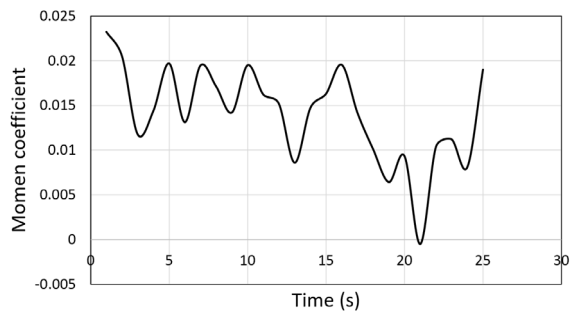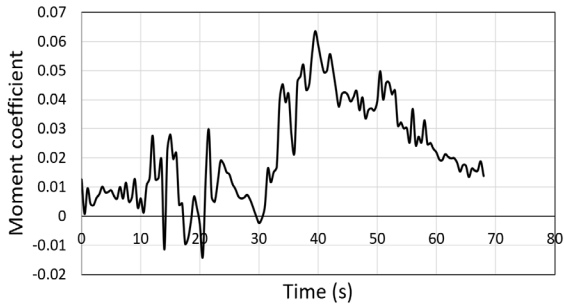


a) Moment coefficient about the X axis



b) Moment coefficient about the Y axis
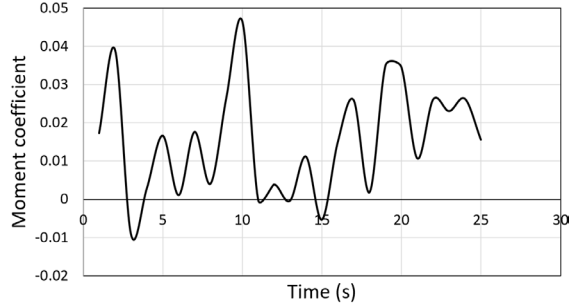


b) Moment coefficient about the Y axis
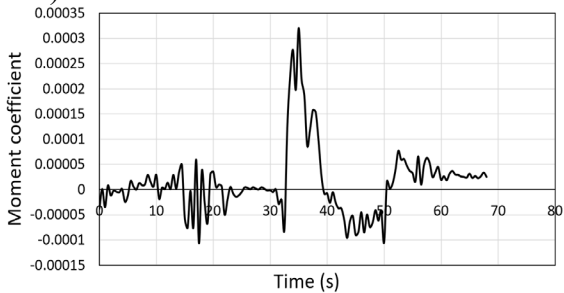


c) Moment coefficient about the Z axis

Figure 3.12 Time history of moment coefficients acting on the FEM under tornadic winds



c) Moment coefficient about the Z axis

Figure 3.13 Time history of moment coefficient acting on the FEM under the equivalent straight-line winds

25

Chapter 4 Modification of the Wind Pressure Equation in AASHTO

The AASHTO Bridge Design Specifications (American Association of State Highway and Transportation Officials 2017) now govern the design of bridges under wind loads. From this standard, the design wind pressure $P_D$ is computed as
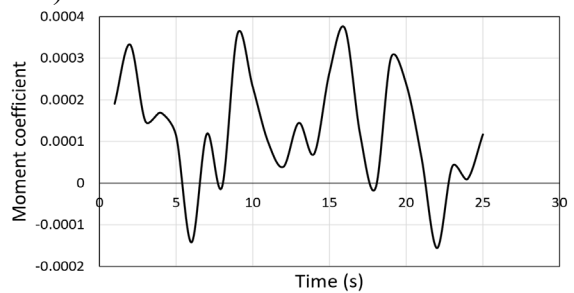
$$P_D = P_B \frac{V_{DZ}^2}{V_B^2} = P_B \frac{V_{DZ}^2}{10000} \left(\frac{kip}{ft^2}\right) \tag{4.1}$$

where the base wind pressure is $P_B = 0.05$ ksf, $V_B = 100$ mph, and $V_{DZ}$ is the design velocity at a particular elevation.

Equation (4.1) is based on the wind pressure caused by straight-line winds. The wind effects of tornadoes are entirely different from those caused by straight-line winds, according to the research findings from earlier chapters; hence, it is not possible to compute the wind pressure caused by tornadoes using Eq. (4.1). In fact, the most recent edition of the AASHTO Bridge Design Specifications, the 8th Edition, which was released in 2017, does not include tornadic wind stresses as a design load. The present AASHTO wind design criteria need to be updated to improve the safety of bridges during tornadoes.

The identical $V_{DZ}$ (81.1 m/s at 6.85 m height) is applied in both tornadic and equivalent straight-line winds in this investigation, and the maximum force coefficients on the bridge are compared. The relationship between the pressure on the bridge under tornadic winds and its equivalent straight-line winds may be seen in the comparison of the force coefficients, as the force is determined by the pressure acting on the entire bridge.

The X direction is the bridge's longitudinal direction, the Y direction is perpendicular to the bridge's longitudinal direction on the horizontal plane, and the Z direction is the vertical direction, as seen in Figure 1.7. The highest magnitude is always attained in the tornadic

scenario, with the exception of the force coefficient in the Y direction, when comparing the force coefficient on the cable-stayed bridge under tornadic winds with the equivalent straight-line winds. Because the wind flow in a straight-line wind field flows perpendicular to the X direction, the wind force is relatively small along the X direction, which is why the peak value of the force coefficient in the X direction under tornadic winds (2.8) is 11 times bigger than that under straight-line winds (0.25). When tornadic winds are present, the force coefficient in the Z direction peaks at 0.25, which is 11 times higher than when straight-line winds are present (0.022). As a result, while designing a cable-stayed bridge to withstand tornadic winds, the wind design should increase the lift force. The highest value of Fz during tornadic winds (0.34) is 7.5 times bigger than that under corresponding straight-line winds (0.045) for the force coefficient acting on the FEM. As a result, it is possible to alter the current wind pressure equation by adding a coefficient, as shown below:

$$P_D = 11 P_B \frac{V_{DZ}^2}{V_B^2} = 11 P_B \frac{V_{DZ}^2}{10000} \left(\frac{kip}{ft^2}\right) \tag{4.2}$$

where $P_B$ = 0.05 ksf, $V_B$ = 100 mph, and $V_{DZ}$ is the design velocity at a particular elevation. Further study may be needed to refine this modification.

Chapter 5 Conclusions and Future Work

The goal of this project is to obtain the wind effects of tornadoes on cable-stayed bridges using computational fluid dynamics (CFD) simulations and to update the equations in AASHTO for calculating the design wind pressure in order to improve the resistance of cable-stayed bridges to tornadoes.

The research outcomes include: 1) A high-fidelity CFD model to determine the wind pressure distribution caused by tornadoes on the cable-stayed bridge; 2) Wind effects acting on the cable-stayed bridge under tornadic winds and under the equivalent straight-line winds; and 3) A revised formula for estimating wind pressure for a tornado-resistant bridge design. Eventually, the design theory of highway bridges based on a thorough comprehension of tornadic wind effects will be advanced by this research.

This project is the second phase of the research, with results based on a historical tornado and a particular cable-stayed bridge. In the future, systematic simulations will be carried out for parametric studies; in addition, studies will be conducted to examine how the current trend will change if the two-way fluid-solid-interaction simulation is applied, when the deformation of the cable-stayed bridge is taken into account. The AASHTO wind pressure equation can then be further modified by adding the amplification coefficient to address more complex scenarios.

References

1. Burgess, D. W. (2006, November). The Tri-State Tornado of 18 March 1925, Part I: Re-examination of the damage path. In *23rd Conference on Severe Local Storms*.

2. Brooks, H. E., & Doswell III, C. A. (2002). Deaths in the 3 May 1999 Oklahoma City tornado from a historical perspective. *Weather and Forecasting*, *17*(3), 354-361.

3. Paul, B. K., & Stimers, M. (2012). Exploring probable reasons for record fatalities: the case of 2011 Joplin, Missouri, Tornado. *Natural hazards*, *64*(2), 1511-1526.

4. Leech, T.G., McHugh, J.D., & Dicarlantonio, G. (2005). Lessons from the Kinzua. *Civil Engineering*, 56-61.

5. Bai, Y., Sun, D., & Lin, J. (2010). Three dimensional numerical simulations of long-span bridge aerodynamics, using block-iterative coupling and DES. *Computers & Fluids*, *39*(9), 1549-1561.

6. Larsen, A. (1998). Advances in aeroelastic analyses of suspension and cable-stayed bridges. *Journal of Wind Engineering and Industrial Aerodynamics*, *74*, 73-90.

7. Bienkiewicz, B. (1987). Wind-tunnel study of effects of geometry modification on aerodynamics of a cable-stayed bridge deck. *Journal of Wind Engineering and Industrial Aerodynamics*, *26*(3), 325-339.

8. Billah, K. Y., & Scanlan, R. H. (1991). Resonance, Tacoma Narrows bridge failure, and undergraduate physics textbooks. *American Journal of Physics*, *59*(2), 118-124.

9. Bosch, H. R. (1978). *Aerodynamic investigations of the Luling, Louisiana cable-stayed bridge* (No. FHWA-RD-77-161 Final Rpt.).

10. Cao, B., & Sarkar, P. P. (2015). Numerical simulation of dynamic response of a long-span bridge to assess its vulnerability to non-synoptic wind. *Engineering Structures*, *84*, 67-75.

11. Cao, J., Ren, S., Cao, S., & Ge, Y. (2019). Physical simulations on wind loading characteristics of streamlined bridge decks under tornado-like vortices. *Journal of Wind Engineering and Industrial Aerodynamics*, *189*, 56-70

12. Conti, E., Grillaud, G., Jacob, J., & Cohen, N. (1996). Wind effects on the Normandie cable-stayed bridge: Comparison between full aeroelastic model tests and quasi-steady analytical approach. *Journal of wind engineering and industrial aerodynamics*, *65*(1-3), 189-201.

13. Diana, G., Yamasaki, Y., Larsen, A., Rocchi, D., Giappino, S., Argentini, T., ... &

Portentoso, M. (2013). Construction stages of the long span suspension Izmit Bay Bridge: Wind tunnel test assessment. *Journal of Wind Engineering and Industrial Aerodynamics*, *123*, 300-310.

14. Kim, B. C., & Yhim, S. S. (2014). Buffeting analysis of a cable-stayed bridge using three-dimensional computational fluid dynamics. *Journal of Bridge Engineering*, *19*(11), 04014044.

15. Kim, B. C., & Yhim, S. S. (2014). Buffeting analysis of a cable-stayed bridge using three-dimensional computational fluid dynamics. *Journal of Bridge Engineering*, *19*(11), 04014044.

16. Hangan, H., & Kim, J. D. (2008). Swirl ratio effects on tornado vortices in relation to the Fujita scale. *Wind and Structures*, 11(4), 291-302.

17. Li, Z., Honerkamp, R., Yan, G., & Feng, R. (2020). Influence of a community of buildings on tornadic wind fields. *Wind and Structures*, *30*(2), 165-180.

18. Franke, J. (2006, July). Recommendations of the COST action C14 on the use of CFD in predicting pedestrian wind environment. In *The fourth international symposium on computational wind engineering, Yokohama, Japan* (pp. 529-532).

19. Erdem, S., Yağmuroğlu, İ., & Saifullah, K. (2016). Assessment of aerodynamic response of the Nissibi cable-stayed bridge using three-dimensional computational fluid dynamics. *CHALLENGE*, *2*(4), 196-204.